Pergamon

doi:10.1016/j.gca.2003.07.012

Pb diffusion in monazite: A combined RBS/SIMS study

D. J. Cherniak,[1,*] E. Bruce Watson,[1] Marty Grove,[2] and T. Mark Harrison[3]

[1]Department of Earth and Environmental Sciences, Rensselaer Polytechnic Institute, Troy, NY 12180 USA
[2]Department of Earth and Space Sciences, University of California, Los Angeles, Los Angeles, CA 90095 USA
[3]Research School of Earth Sciences, Australian National University, Canberra, ACT 0200 Australia

Abstract—We report measurements of Pb diffusion in both synthetic ($CePO_4$) and natural monazites run under dry, 1-atm conditions. Powdered mixtures of prereacted $CePO_4$ and $PbZrO_3$ were used as the source of Pb diffusant for "in-diffusion" experiments conducted in sealed Pt capsules for durations ranging from a few hours to several weeks. Following the diffusion anneals, Pb concentration profiles were measured with Rutherford Backscattering Spectroscopy (RBS) and supplemented by measurements with secondary ion mass spectrometry (SIMS). In order to evaluate potential compositional effects upon Pb diffusivity and simulate diffusional Pb loss that might occur in natural systems, we also conducted "out-diffusion" experiments on Pb-bearing natural monazites. In these experiments, monazite grains were surrounded by a synthetic zircon powder to act as a "sink." Monazites from these experiments were analyzed with SIMS. Over the temperature range 1100 to 1350°C, the Arrhenius relation determined for in-diffusion experiments on synthetic monazite is given by:

$$D = 0.94 \exp\left(-592 \pm 39 \text{kJ mol}^{-1}/RT\right) \text{m}^2 \text{ s}^{-1}$$

Diffusivities for synthetic and natural monazites are similar, as are results of measurements made on the same samples using both RBS and SIMS. The activation energy for Pb diffusion we determined is more than three times that for natural monazite reported previously, with Pb diffusivities at <1200°C significantly lower than those earlier reported but similar to that of zircon. Our data indicate that a 10-μm-sized monazite grain would have a Pb closure temperature in excess of 900°C, given a cooling rate of 10°C/Ma. Clearly, other factors may affect U-Th-Pb systematics in monazite including possible nondiffusive effects such as recrystallization mediated by fluids or triggered by metamorphic reactions with other REE-bearing minerals. However, our data suggest that monazite may be quite resistant to alteration of Pb isotopes by the specific mechanism of solid-state diffusional exchange. *Copyright © 2004 Elsevier Ltd*

1. INTRODUCTION

Monazite is widely used for U-Pb geochronology in rocks from moderate to high-grade metamorphic terranes, and is important because it grows as a metamorphic mineral over a broad stability range (see review in Harrison et al., 2002). It also possesses high closure temperature, although some controversy remains regarding the appropriate range for values of T_c. Further, despite typically high Th and U contents (~1–25 and 0.01–1 wt%, respectively) monazites frequently yield concordant ages in the U-Pb system without evidence of Pb loss that is characteristic of zircons (e.g., Parrish, 1990), presumably because of the greater resistance of monazite to radiation damage effects as compared with zircon (e.g., Meldrum et al., 1998) and associated Pb mobility enhanced by crystal lattice damage (e.g., Cherniak et al., 1991; Cherniak, 1993). However, in many ways the U-Th-Pb system in monazite is complex (e.g., Zhu et al., 1997; Bingen and Van Breemen, 1998). Distinct age and/or compositional domains in monazites are frequently observed, and it has been established that recrystallization, generally mediated by fluids, can effect the U-Th-Pb system in monazite (e.g., Teufel and Heinrich, 1997; Townsend et al., 2001). It is therefore essential to assess and elucidate the contribution of diffusion to U-Th-Pb systematics by direct measurement of Pb diffusion over a broad range of conditions.

We report here our findings on Pb diffusion in both natural and synthetic monazites. These data further complete the picture for Pb diffusion in accessory minerals and indicate that monazite is to date the most retentive of Pb under experimental conditions. Since many factors have the potential to influence diffusion rates, we investigate the effects of several parameters on Pb diffusion. In the set of experiments described below, we consider cases of out- and in-diffusion, and the potential effect of composition of synthetic and natural monazites on diffusivities. We also use two different analytical techniques, RBS and SIMS, to measure Pb concentration profiles. The consistency of these findings over this range of conditions suggests to that our result provides the best basis to assess the natural behavior of Pb diffusion in monazite.

2. MATERIALS AND METHODS

2.1. In-Diffusion Experiments

2.1.1. Monazite synthesis, source, and sample preparation

The synthetic monazites used in this study were grown at 1.0 GPa in a solid medium piston cylinder apparatus. The method, adapted from procedures of Montel (1989) and Anthony (1957, 1964), uses a cerium hydroxide gel and phosphoric acid solution. The cerium hydroxide gel was synthesized by dissolving cerium ammonium nitrate in distilled water in a teflon beaker. Ammonium hydroxide was added to the solution to form a light yellow precipitate. The gel was dried at ~80°C for a few hours in a drying oven, then dried at room temperature overnight. It was then ground and placed in the drying oven for a few days, and was finally reground. The dried gel was combined with 85%

* Author to whom correspondence should be addressed (chernd@rpi.edu).

Table 1. Compositional analysis of natural monazite (Hiddenite, NC) used in this study (determined by electron microprobe analysis).

Oxide	wt%
P_2O_5	30.04
SiO_2	0.26
CaO	0.01
PbO	0.01
ThO_2	0.02
UO_2	0.14
Y_2O_3	0.77
La_2O_3	15.65
Ce_2O_3	31.79
Pr_2O_3	3.31
Nd_2O_3	12.97
Sm_2O_3	2.53
Gd_2O_3	1.81
Tb_2O_3	0.15
Dy_2O_3	0.43
Er_2O_3	0.04
Total	100.29

H_3PO_4 solution in the ratio of 3 g gel to 1 mL solution, and loaded into a Pt capsule inserted either in alumina or an oxidized Ni capsule. The syntheses were run in piston-cylinder apparatus at 1.0 GPa for 3 d. Two separate runs at 1000 and 1100°C, respectively, yielded well-formed monazite crystals up to a few mm in length and pale green in color.

Synthetic monazites with relatively large growth faces ({100}) were selected for in-diffusion anneals, and underwent no further surface preparation beyond ultrasonic cleaning in baths of distilled water and ethanol. To investigate whether differences in trace-element compositions or defect concentrations influence Pb diffusion in monazite, experiments were also run on a natural monazite from Hiddenite, North Carolina (now popularly referred to as the "eBay monazite" because of its purchase through a well-known online auction site). Compositional information for this monazite is provided in Table 1. These specimens were well-formed crystals a few mm on a side possessing large natural growth faces. Crystals with good growth faces ({100}) with areas greater than 1 mm² were chosen for in-diffusion experiments and underwent no surface preparation other than ultrasonic cleaning. To investigate anisotropy of Pb diffusion, specimens of the natural monazite with good (110), (101), and (−111) growth faces were selected. The samples then were preannealed at 1200°C in air overnight.

For out-diffusion experiments on natural monazite, both natural growth faces and polished sample surfaces of the North Carolina monazite were used. The polished samples were polished with SiC paper down to 600 grit, then with alumina down to 1 μm, and finally with colloidal silica. Additional out-diffusion experiments were run on 554 monazite, from the Santa Catalina Mountains, Arizona, used as a standard in Th-Pb ion microprobe analyses of monazite (Harrison et al., 1999a). Compositional data for 554 is given in Catlos et al. (2002). As with the North Carolina monazite, both polished and natural surfaces were used in experiments. Because of the small size of the 554 monazites used (at most a few hundred microns in length) they were polished by mounting in an epoxy disk, and extracted from the mount following polishing by thinning the disk to about one mm thickness, then slightly warming and bending the disk to release the grains.

The source of diffusant consisted of a mixture of $PbZrO_3$ and $CePO_4$ powders in 1:3 weight ratio. The source constituents were mixed, placed in a covered Pt crucible, and heated in air overnight at 1250°C, then reground. Powdered or ground materials have been employed as sources of diffusant in numerous studies (e.g., Cherniak and Watson, 1992, 1994; Cherniak et al., 1997a,b; Watson and Cherniak, 1997) and have yielded diffusivities comparable to those obtained through techniques introducing diffusants by other means (e.g., Derry et al., 1981; Watson et al., 1985; Cherniak and Watson, 1992, 1994; Cherniak and Ryerson, 1993; Giletti and Casserly, 1994; Moore et al., 1998; Hammouda and Cherniak, 2000). The numerous point contacts of the source powders (and the sink materials described in later sections) provide essentially continuous surface coverage given the experimental geom-

etry and the relative rapidity of grain boundary and surface diffusion (e.g., Tannhauser, 1956; Gjostein, 1973).

2.1.2. One atmosphere experiments

Experiments were run at one atmosphere by placing the monazite and source in a Pt capsule (3 mm od) and welding shut. Prepared capsules were then annealed at temperatures ranging from 1100 to 1350°C and times ranging from 5 h to 2.5 months (Table 2). Experiments were run in vertical tube furnaces with $MoSi_2$ heating elements, and temperatures monitored with Pt-Pt10%Rh (type S) thermocouples. Temperature uncertainties were about ±2°C. Following diffusion anneals, experiments were quenched by removing from furnaces and permitting capsules to cool in air. A "zero-time" anneal was also performed, to assess the likelihood of nondiffusional uptake of Pb during the heatup and quench phases of the anneal, and to explore the possibility of other difficulties with the experimental approach. For the "zero time" run, a sample capsule was prepared as described above for 1-atm experiments, using a synthetic monazite. The capsule was then brought up to run temperature (1300°C) and immediately quenched.

2.2. Out-Diffusion Experiments

Out-diffusion experiments were done with the natural North Carolina and 554 monazites. Prepared monazites were annealed in Pt capsules surrounded by finely powdered synthetic zircon (made through solid-state reaction of SiO_2 and ZrO_2 powders) as a sink for Pb. Other sink materials were tried (including a synthetic $CePO_4$ powder), but were found to react with the sample surface during diffusion anneals at high temperature; experiments run with the zircon displayed no evidence of this surface alteration. Profiles from out-diffusion experiments were measured with SIMS.

2.2.1. RBS analysis

RBS has been used in many diffusion studies (e.g., Cherniak and Watson, 1992, 1994; Cherniak, 1995) and the experimental and analytical approach used here is similar to that taken previously. Analyses typically employed ⁴He⁺ beams of energies of either 2 or 3 MeV, with beam spot size typically ∼1mm². Spectra were converted to Pb concentration profiles using procedures outlined in publications cited above.

The RBS profiles measured following diffusion anneals were fit with a model to determine the diffusion coefficients (*D*). In-diffusion is modeled as simple one-dimensional, concentration independent diffusion in a semi-infinite medium with a source reservoir maintained at constant concentration (i.e., a complementary error function solution). The rationale for the use of this model has been elsewhere discussed (e.g., Cherniak and Watson, 1992, 1994; Cherniak, 1993). Diffusivities are evaluated by plotting the inverse of the error function (i.e., erf^{-1} $((C_o - C(x, t))/C_o)$ vs. depth (*x*) in the sample. A straight line of slope $(4Dt)^{-1/2}$ will result if the data satisfy the conditions of the model. C_o, the surface concentration of diffusant, is independently determined by iteratively varying its value until the intercept of the line converges on zero. In Figure 1, typical in-diffusion profiles and their inversions through the error function are shown. The uncertainties in concentration and depth from each data point (mainly derived from counting statistics in the former and detector resolution and energy spread of the analyzing ion beam in the latter) were used to evaluate the uncertainties in the diffusivities determined from the fits to the model.

2.2.2. SIMS analyses

During SIMS analysis, virtually all secondary ions originate from the first couple of atomic layers of the instantaneous sample surface. Thus atomic mixing due to the impacting primary ions, geometric effects on crater production, and correction for surface correlated Pb are the essential limiting factors on depth resolution. These effects require that the measured diffusion profile extend over a depth of >50 nm. Details of analytical protocols for depth profiling analysis of Pb in monazite using the CAMECA ims 1270 ion microprobe are given in Grove and Harrison (1999). To briefly summarize, a mass resolving power of 4500

Table 2. Pb diffusion in monazite.

	T(°C)	Time (s)	D(m²s⁻¹)	log D	±	Analysis
			Synthetic monazite (CePO₄) (normal to (100) face)			
syn2	1350	4.93×10^5	2.3×10^{-20}	−19.6	0.3	SIMS
PbEBWM-12	1348	1.80×10^4	5.74×10^{-20}	−19.24	0.23	RBS
PbEBWM-15	1300	3.24×10^4	2.63×10^{-20}	−19.58	0.20	RBS
PbEBWM-11	1301	8.10×10^4	2.95×10^{-20}	−19.53	0.23	RBS
PbEBWM-14	1300	3.30×10^5	1.94×10^{-20}	−19.71	0.16	RBS
PbEBWM-10	1253	2.27×10^5	6.71×10^{-21}	−20.17	0.16	RBS
syn10	1250	2.27×10^5	2.8×10^{-20}	−19.55	0.11	SIMS
PbEBWM-9	1250	2.30×10^5	3.24×10^{-21}	−20.49	0.18	RBS
PbEBWM-8	1201	3.13×10^5	1.15×10^{-21}	−20.94	0.17	RBS
syn8	1200	3.49×10^5	6.0×10^{-21}	−20.22	0.15	SIMS
PbEBWM-13	1151	1.70×10^6	1.49×10^{-22}	−21.83	0.19	RBS
PbEBWM-13b	1151	1.70×10^6	1.11×10^{-22}	−21.95	0.26	RBS
PbEBWM-17	1100	6.67×10^6	4.33×10^{-23}	−22.36	0.25	RBS
			Natural monazite (normal to (100) face)			
PbNCMz-3	1350	2.16×10^4	3.73×10^{-20}	−19.42	0.22	RBS
Ebay4	1300	4.03×10^5	6.0×10^{-20}	−19.22	0.12	SIMS
PbNCMz-2	1300	1.08×10^5	1.34×10^{-20}	−19.87	0.15	RBS
PbNCMz-1	1249	3.38×10^5	3.63×10^{-21}	−20.44	0.18	RBS
Ebay8	1249	1.20×10^5	1.1×10^{-20}	−19.96	0.19	SIMS
			Normal to (−111) face			
PbNCMz-10	1250	2.54×10^5	5.36×10^{-21}	−20.27	0.12	RBS
			Normal to (101) face			
PbNCMz-11	1250	2.54×10^5	4.07×10^{-21}	−20.39	0.13	RBS
			Normal to (110) face			
PbNCMz-12	1250	2.54×10^5	5.03×10^{-21}	−20.30	0.26	RBS

adequately separates all molecular interferences in the 204 to 208 mass range in monazite. In the depth profile mode, we use a $\sim 30~\mu m$ primary O⁻ beam to sputter the monazite target. To minimize mixing of secondary ions derived from different depths close to the crater edge, we used a $\sim 100~\mu m$ field aperture to restrict entry into the mass spectrometer to only those ions originating on the crater floor. We limited the depth/diameter ratio of the sputtered craters to <0.1 to minimize variations in the sputtering conditions at the sample surface. Subsequent to analysis, pit dimensions were measured using a DekTak© surface profilometer with a nominal precision of ±50 Å. By measuring excavation depth as a function of time, it was determined that a $\sim 30~\mu m$ diameter, 4 nA O⁻ primary beam removed material from unpolished 554 monazite at 1 to 1.5 $\mu m/h$. Crater depths were calculated from this relationship after normalizing for variations in primary beam current and preanalysis sputtering duration. Pre and postanalysis measurement of the primary beam current indicated that drift was generally <1%/h while the duration of preanalysis sputtering required to remove the Au coat and perform peak centering was 2–3 min.

For the out-diffusion experiments using the North Carolina and 554 monazites, a initial uniform concentration of ²⁰⁸Pb in the monazite was assumed (see Grove and Harrison, 1999), with the concentration of Pb in the surrounding medium essentially zero. For the in-diffusion experiments using the Ce-monazite, a initial uniform ratio of ²⁰⁸Pb/ ¹⁴⁰CePO₂ is assumed.

For one-dimensional, concentration-independent out-diffusion, the solution to the diffusion equation is $C = C_o erf(x/(4Dt)^{1/2})$, where C_o is the initial concentration of Pb in the monazite (Crank, 1975). A typical Pb in-diffusion profile, obtained with SIMS, is shown in Figure 2 together with the fitted error-function curve that is the solution to the diffusion equation.

3. RESULTS

The results for Pb diffusion in monazite are presented in Table 2 and plotted in Figure 3. A least-squares linear fit to the in-diffusion data (Fig. 3) for synthetic monazite (RBS measure-

ments only) yields an activation energy for diffusion of 594 ± 39 kJ mol⁻¹ and preexponential factor 9.4×10^{-1} m²s⁻¹ (log $D_o = -0.028 \pm 0.014$) for diffusion normal to the (100) face. A time-series of anneals run at 1300°C (Fig. 4) indicates that Pb diffusion is independent of time for durations differing by about an order of magnitude. Diffusion anneals at 1250°C for (110), (101) and (−111) faces (with diffusivities measured normal to these faces) of the natural North Carolina monazite yielded diffusivities indistinguishable from those measured normal to the (100) face, indicating little anisotropy for Pb diffusion in monazite. This contrasts somewhat with the finding of Smith and Giletti (1997), who suggest that diffusion perpendicular to c is the fastest, with diffusion along the c-axis 2 to 5 times slower.

Although no experiments were done to explore Pb diffusion under hydrothermal conditions, it is unlikely that the presence of water would substantially affect volume diffusion rates. In those cases where cation diffusion has been measured under both wet and dry conditions for both silicates (e.g., Cherniak and Watson, 2001) and phosphates (e.g., Cherniak and Ryerson, 1993; Farver and Giletti, 1998), no significant difference has been documented.

The good agreement of Pb diffusion results obtained for in-diffusion in the natural monazites with those for the synthetic monazite suggests that even relatively large differences in monazite composition have little effect on Pb diffusion. A fit of all of the in-diffusion data for both synthetic and natural monazite (RBS measurements only) yield an activation energy of 563 ± 35 kJ mol⁻¹ and preexponential factor 0.089 m²s⁻¹ (log $D_o = -1.05 \pm 1.20$), in agreement within uncertainty of the above diffusion parameters for the synthetic monazite only.
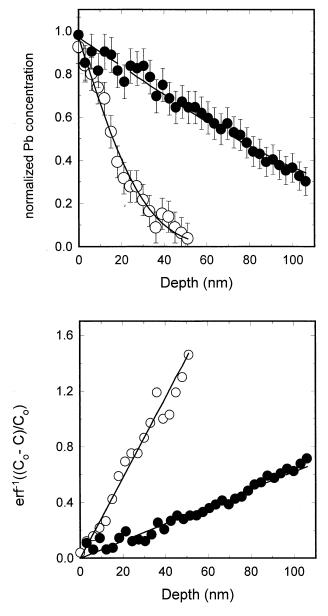
Fig. 1. Typical diffusion profiles for Pb in-diffusion experiments in synthetic (dark circles = sample PbEBWM-14) and natural (open circles = sample PbNCMz-2) monazite measured by RBS. (a) The diffusion data are plotted with complementary error function curves. (b) The data are inverted through the error function. Slopes of lines are equal to $(4Dt)^{-1/2}$.

Fig. 2. Pb diffusion profile for in-diffusion in a synthetic monazite, measured by SIMS. The curve is a fit to the data with the model outlined in the text.

Diffusion coefficients derived from SIMS measurements of both in- and out-diffusion experiments (1200 to 1300°C) plot near the RBS results, with the majority about half a log unit above the Arrhenius relationship presented in the previous paragraph (Fig. 3). The in-diffusion datum at 1350°C plots below that line. A fit to all of the data for both natural and synthetic monazite, in-diffusion and out-diffusion experiments, measured with RBS and SIMS, yields an activation energy of 536 ± 51 kJ mol^{-1} and preexponential factor 1.4×10^{-2} m^{2}s^{-1} (log $D_o = -1.860 \pm 1.757$), in agreement within uncertainty with the Arrhenius parameters presented above for the RBS

results. While the SIMS data broadly confirm the RBS results, differences between the two analysis methods are expected due to the differing lateral resolution each brings to the problem. The RBS method averages over $\sim$mm^2 areas while SIMS interrogates a region that is about a thousand times smaller. While near continuous surface coverage of the diffusant source is satisfactory for RBS analysis, small regions where source contact is not made will not show significant Pb penetration when analyzed by the SIMS depth profiling method. Furthermore, relatively small cracks which transect the analyzed surface can locally carry diffusant into the crystal by grain boundary diffusion potentially yielding higher apparent diffusivities. The resulting profiles can be recognized by their lack of fit to an error function. Both behaviors (i.e., no profile and anomalously long non-Fickian profiles) were encountered during SIMS depth profiling. Only those profiles which conformed to the expected error function shape were used for calculating diffusion coefficients. Quoted uncertainties reflect the standard deviation calculated for between six to eight individual profiles. The in-diffusion result at 1350°C was exceptional in yielding a very broad spectrum of apparent diffusivities.

In addition to the isothermal time series, a "zero time" experiment provides another means by which we can affirm that what we are measuring is in fact volume diffusion. The lack of a significant amount of Pb uptake or near-surface exchange in the "zero time" run (not shown; Table 2) suggests that rapid surface reaction during the initial stages of the anneal does not contribute substantially to observed Pb profiles in the diffusion experiments.

4. DISCUSSION

4.1. Previous Measurements of Pb Diffusion in Monazite

In an early experimental study of sintered monazite, Shestakov (1969) estimated an activation energy of 250 kJ mol^{-1} by volatilizing Pb in a stream of nitrogen at temperatures between
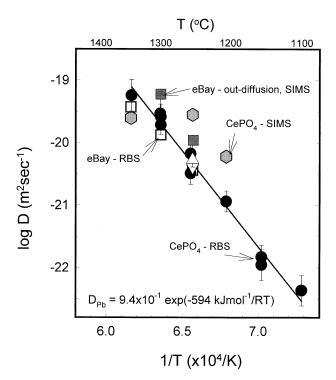
Fig. 3. Arrhenius plot of Pb diffusion in monazite. Plotted are in-diffusion experiments on synthetic and natural monazite, measured with both RBS (solid circles and white squares for synthetic and natural monazite, respectively) and SIMS (gray hexagons), and out-diffusion experiments on natural monazite (gray squares) measured by SIMS. These data are for diffusion normal to the (100) face. White and gray triangles are for in-diffusion in natural monazite normal to (−111), (101) and (110) faces. The line is a least-squares fit to the in-diffusion data for synthetic monazite. Arrhenius parameters extracted from the fit are: activation energy 594 ± 39 kJ mol^{-1} and preexponential factor 0.94 m^{2}s^{-1} (log D_o = −2.783×10^{-2} ± 1.350).
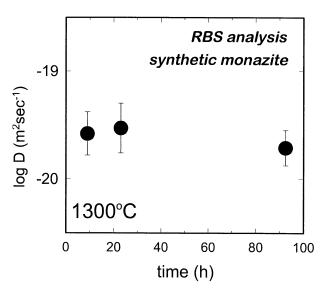

Fig. 4. Time series for Pb diffusion anneals of synthetic monazite. Diffusivities at 1300°C are generally quite similar for anneal times differing by a factor of about an order of magnitude, indicating that what is being measured is volume diffusion.

800 to 1100°C. Smith and Giletti (1997) measured diffusion of Pb in natural monazite at temperatures 1000–1200°C at 1 atm using a ^{204}Pb tracer applied to sample surfaces, with depth profiling done by SIMS (Fig. 5). They obtained an activation energy of 180 ± 48 kJ mol^{-1} and preexponential factor of 6.6 × 10^{-15}m^{2}s^{-1}. Suzuki et al. (1994) estimated Pb diffusivities in natural monazite by measuring Pb gradients in monazite grains from paragneiss samples from the Ryoke metamorphic belt (Fig. 5). They calculated diffusivities of 1.9 × 10^{-25} m^{2}s^{-1} at 620°C and 1.5 × 10^{-24} m^{2}s^{-1} at 680°C, and esti- mated an activation energy for diffusion of 244 kJ mol^{-1} and preexponential factor of 3.4 × 10^{-11} m^{2}s^{-1}. All these activa- tion energies are significantly lower than that obtained in the present study, which has significant implications for the mo- bility of Pb at lower temperatures. In the temperature range over which this work and the study of Smith and Giletti (1997) overlap, diffusivities at the highest temperature at which they measured Pb diffusion (1200°C) are quite similar to those we have determined. At 1100°C, however, our measured diffusivi- ties are about an order of magnitude lower than those in Smith and Giletti's work. It is not clear why this discrepancy exists, but analytical artifacts may be responsible. The activation en- ergy determined by Smith and Giletti (1997) is anomalously low (see Dahl, 1997) and not well-constrained, since there is

considerable scatter (about an order of magnitude in each case) among diffusivities measured at both the highest (1200°C) and lowest (1000°C) temperatures investigated.

Our findings also differ dramatically from Pb diffusivities estimated by Suzuki et al. (1994). Extrapolating down-temper- ature using our Arrhenius relation, we obtain diffusivities that are 8 to 9 orders of magnitude lower than that the Suzuki et al. (1994) estimates. While there is some uncertainty associated with down-temperature extrapolation, it is unlikely that such a large discrepancy can be explained merely by this given the constraints on our Arrhenius parameters. It is perhaps the case that Pb gradients measured on the monazite grains studied by Suzuki et al. (1994) have resulted from processes other than simple volume diffusion.

4.2. Pb Diffusion in Other Minerals

There now exist measurements of Pb diffusion in a range of minerals, including those in other accessory minerals employed in U-Th-Pb geochronometry. A summary of these data is given in Figure 6. It is evident from this compilation that diffusion of Pb in monazite is very slow with respect to other minerals (with the exception of zircon) for which Pb diffusion has been determined. This is consistent with the observation that mon- azite can be quite resistant to thermal disturbance (e.g., Harri- son et al., 1997; Hawkins and Bowring, 1997; Zhu et al., 1997; Schmitz and Bowring, 2003). The high activation energy and low diffusivity for Pb diffusion in monazite are also consistent with observed trends showing negative correlations of diffu- sivities at metamorphic temperatures and activation energies for diffusion with mineral ionic porosities (e.g., Dahl, 1997) and positive correlations with elastic parameters (e.g., Cher- niak, 1998).

Perhaps most interesting is the similarity of Pb diffusivities in monazite and zircon. Activation energies for diffusion in
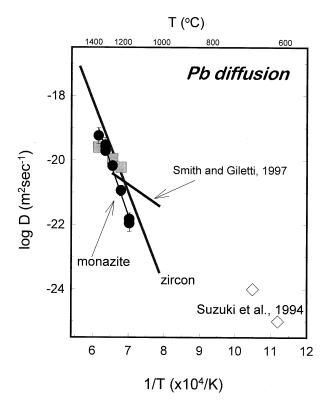
Fig. 5. Summary of measurements of Pb diffusion in monazite. Sources for data are noted on the graph. The present work indicates a significantly larger activation energy for diffusion than earlier studies, suggesting very slow diffusivities for Pb for temperatures below 1000°C.
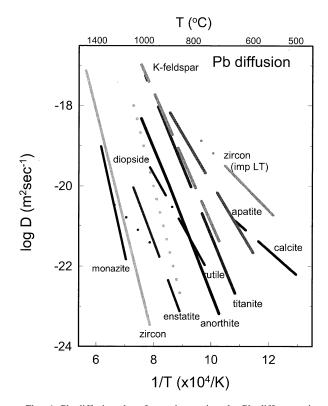

Fig. 6. Pb diffusion data for various minerals. Pb diffuses quite slowly in monazite compared with most minerals for which diffusion data exist, with the exception of zircon. Sources for data: anorthite, K-feldspar = Cherniak (1995); apatite = Cherniak et al. (1991); calcite = Cherniak (1997); diopside = Cherniak (1998); enstatite = Cherniak (2001); rutile = Cherniak (1998); titanite = Cherniak (1993); zircon = Cherniak and Watson (2001).

both minerals are comparable, at 592 ± 39 for monazite vs. 550 ± 30 kJmol^{-1} for zircon, and measured diffusivities overlap in the temperature range 1100–1350°C. Hence, monazite and zircon would be predicted to close to Pb exchange at about the same temperature, and thus could be expected to be similarly robust geochronometers under some conditions. However, differences in the response of these minerals to geological conditions may lead to varying patterns of discordance for each.

4.3. Calculated Closure Temperatures

We can use our experimentally-determined Pb diffusion parameters to calculate Pb closure temperatures for monazite as a function of effective diffusion radius and cooling rate, and these values can be compared with field based estimates of T_c. The closure temperature equation (Dodson, 1973) is:

$$\frac{E}{RT_c} = \ln\left(\frac{ART_c^2 D_0/r^2}{E\ dT/dt}\right) \quad (1)$$

where E and D_o are the activation energy and preexponential factors for diffusion of the relevant species, dT/dt is the cooling rate, r is the effective diffusion radius, and A is a geometric factor. The derivation of the above expression rests on several assumptions (Dodson, 1973, 1986); among these is the condition that at peak temperature T_o, the mineral grain is not retentive of the daughter product over short timescales. This

assumption, which makes T_c independent of T_o, is, as Ganguly et al. (1998) note, not satisfied for slowly diffusing species. Given that diffusion of Pb in monazite appears to be exceedingly slow under crustal conditions, this condition is not satisfied for monazite, nor can it even be assumed that homogeneity is achieved at a peak metamorphic temperatures. However, when the dependence of T_c on T_o is taken into account in calculating closure temperatures, the deviations of T_c from conventional closure temperatures calculated using Eqn. 1 are smaller with increasing peak temperature (T_o) and slower cooling rate (Ganguly et al., 1998; Ganguly and Tirone, 1999). The geometric factor, A, in Dodson's expression of mean closure temperature above, is equal to $exp(G)$, where G is the value of the closure function, $G(x)$, spatially averaged over the crystal. In deriving the expression for $G(x)$, and ultimately A, the dimensionless parameter M (where M is defined as equal to $D(T_o)RT^2/(Er^2 dT/dt)$), is much greater than 1 (Dodson, 1986). For smaller values of M, another term, $g(x)$, will become significant, and is summed with G in the exponential expression above to produce the variable A', where $A' = exp(G(x) + g(x))$, which can be substituted for A in Eqn. 1 above. A' will be larger than the value of 55 (i.e., $exp(4.0066)$) one obtains when the condition of $M \gg 1$ is met (i.e., when $g(x) \rightarrow 0$). With increasing A', closure temperature will exhibit greater deviation from Dodson's (1973) classical formulation.

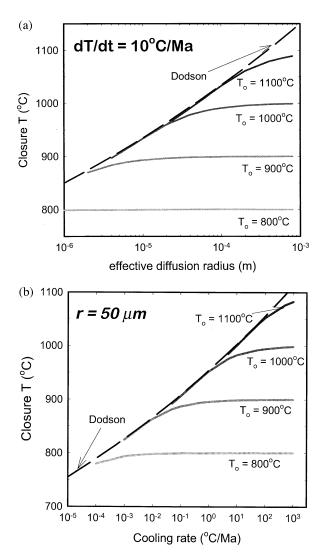This is illustrated in Figure 7, where mean closure temper-

Fig. 7. Mean closure temperatures for Pb in monazite as a function of grain radius with a fixed cooling rate of 10°C/Ma (a), and as a function of cooling rate for a fixed grain radius of 50 μm (b). Closure temperature curves are calculated for a few different peak temperatures (T_o), using the expressions of Ganguly and Tirone (1999), which consider cases of closure with arbitrarily small extent of diffusion. Also plotted are closure temperatures calculated using the classical Dodson (1973) formula (dashed lines). Deviations in mean closure temperatures from the Dodson curves can be observed to increase with larger grain radii, faster cooling rates, and decreasing peak temperatures. Spherical geometry was used in all calculations.
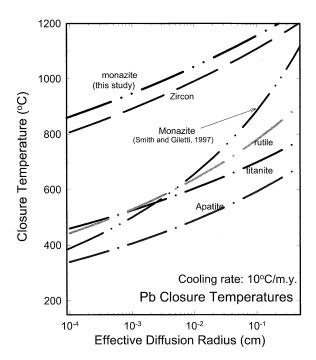

Fig. 8. Closure temperatures for Pb in accessory minerals as function of effective diffusion radius for a cooling rate of 10°C per million years. Calculations were made employing the standard expression of Dodson (Eqn. 1). Sources for diffusion data for closure temperature calculations are included in the caption for Figure 6. Also plotted for comparison are closure temperatures calculated using the diffusion data of Smith and Giletti (1997).

atures for Pb in monazite are plotted as a function of diffusion radius for a cooling rate of 10°C/Ma, and spherical geometry (Fig. 7a). Also plotted (Fig. 7b) are mean closure temperatures as a function of cooling rate for a fixed grain radius (50 μm). In each case, curves for 4 different values of T_o are shown, which have been calculated using the extension of the Dodson formulation from Ganguly and Tirone (1999), using software developed by these authors. These curves are plotted with those calculated using the conventional Dodson (1973) expression (Eqn. 1). For small grain radii, slow cooling rates, and comparatively high peak temperatures, the former closure temperature curves will converge upon the Dodson values, but signif-

icant deviations can exist for larger grains, fast cooling rates, and lower peak temperatures. Given the small grain size of most typical monazites, closure temperatures for Pb may approach the Dodson values under many cooling conditions.

As noted above, closure temperatures calculated using Eqn. 1 are mean values, as closure temperature varies with distance from the crystal surface. However, except for a very narrow outermost layer, closure temperatures will not differ from the mean by more than a few tens of degrees for cooling rates between 1 and 10°C/Ma and grain sizes up to a few mm. For example, for 100 μm radius grains, mean T_c is ~10°C higher than that for a point 10 μm from the surface; T_c for the grain center will be ~40°C higher than the mean value. A point 1 μm from the surface, however, will have a T_c 80–90°C lower than the mean.

It should be clear from the above discussion that T_c is dependent on many factors, and there is no single "closure temperature" for a given mineral. Nonetheless, we can use the simplified expression above to make broad comparisons of closure of Pb in various accessory minerals, and to consider closure temperature values calculated from our diffusion parameters in light of the estimates of closure temperatures for Pb in monazite cited above.

In Figure 8, we plot closure temperature for various accessory minerals as function of effective diffusion radius, using the "classical" closure equation (i.e., Eqn. 1). We plot curves calculated using both the usual geometric factor for spherical geometry (i.e., $A = 55$). Apparent closure temperatures for Pb in monazite are quite high, considerably in excess of those for
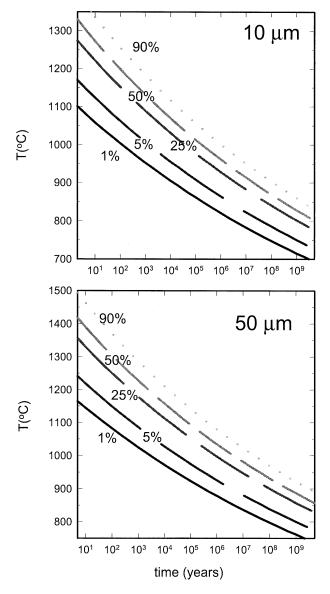
Fig. 9. Conditions for diffusional Pb loss in monazite for grains of effective radii of 10 and 50 μm. Curves represent time-temperature conditions under which monazite will lose the indicated fraction of total Pb. Even small monazite grains will lose negligible (~1%) Pb through diffusion at 700°C for times in excess of a billion years.

other accessory minerals save zircon. For example, T_c for a grain of 10 μm effective radius would be ~950°C, and ~1050°C for 100 μm radius grains (for a cooling rate of 10°C/Ma), values ~50°C higher than zircon. In contrast, T_c calculated for Pb in monazite using the Smith and Giletti (1997) Arrhenius parameters are significantly lower, with monazites of 10 and 100 μm effective diffusion radii closing to Pb exchange at 500 and ~650°C, respectively.

Likewise, we can use our Arrhenius relationship to estimate the degree of exchange of Pb in monazite during isothermal heating episodes. The curves in Figure 9 represent the percentage of Pb loss for monazites of 10 and 50 μm radii when subjected to various time-temperature conditions. These curves are calculated assuming spherical geometry, using the expres-

sions of Crank (1975; section 6.3.1) for fractional loss from a sphere of initial uniform concentration with constant surface concentration. Monazites of 10 μm radius would lose only ~1% of their Pb if residing at 700°C for times on order of the age of the earth; 50 μm monazites would require ~100 m.y. at 800°C to lose 1% of their Pb.

Since the present results suggest that monazite is resistant to Pb loss by volume diffusion alone, we next explore several aspects of the U-Th-Pb monazite dating system, and consider the circumstances under which open-system behavior may occur.

4.4. Open System Behavior in the U-Th-Pb Monazite System

4.4.1. Radiation damage

Radiation damage in minerals accumulates largely from the recoil of the heavy nucleus following alpha decay. Thus it is surprising that although monazite is typically hundreds of times more radioactive than zircon, it does not become metamict. Zircons more readily become metamict when subjected to heavy-ion irradiation, which produces lattice damage comparable to that resulting from alpha recoil events during radioactive decay (e.g., Weber, 1990; Murakami et al., 1991; Weber et al., 1994; Meldrum et al., 1998).

However, the mechanism that is able to naturally restore the monazite structure is poorly understood. Heavy ion implantation experiments show that natural monazite cannot be rendered metamict above 175°C (Meldrum et al., 1997b). For synthetic LaPO$_4$, the threshold temperature is as low as 60°C. Totally amorphous monazite is completely recrystallized by laboratory heating to 300°C (Karioris et al., 1981). Electron irradiation produced during alpha decay may be an efficient way to anneal metamict monazite (Meldrum et al., 1997a). It has been suggested that the strong bonds between P and O and the low symmetry monazite structure may be responsible for the near total resistance of natural monazites to accumulating radiation damage (Cherniak et al., 1991; Cherniak, 1993; Krogstad and Walker, 1994; Meldrum et al., 1996, 1997b).

Pb diffusivities have been found to be considerably faster in both radiation damaged zircon (Cherniak et al., 1991; Cherniak and Watson, 2001) and titanite (Cherniak, 1993) than in their undamaged counterparts. Because phosphates are more resistant to the accumulation of such lattice damage, Pb transport rates in apatite (Cherniak et al., 1991) and monazite are less likely to be affected because these materials may not reach the stage of having sufficient disruption of lattice order to permit enhanced diffusivities.

4.4.2. Monazite dissolution and recrystallization

While there are numerous metamorphic reactions that involve monazite breakdown (Finger et al., 1998; Bea and Montero, 1999; Catlos et al., 2002), our interest here is limited to those cases where a record of the resetting of the U-Th-Pb system in monazite is preserved (e.g., Zhu and O'Nions, 1999a; Townsend et al., 2001).

Recrystallization of monazite can occur as a consequence of coarsening of matrix phases that are held at high temperature for extended periods. When grain boundaries move, accessory

phases tend to move with them by recrystallizing through dissolution and precipitation because it is energetically favorable for them to remain on grain boundaries (Watson et al., 1989). Ostwald ripening can drive dissolution-reprecipitation of monazite (e.g., Kingsbury et al., 1993) until a critical size threshold is exceeded (Ayers et al., 1999).

Several studies suggest that fluid-mediated recrystallization can influence U-Pb discordance patterns in monazite. Teufel and Heinrich (1997) have found efficient resetting of the U-Pb isotope system by dissolution-precipitation under hydrothermal conditions, even at low temperatures. Crowley and Ghent (1999) attributed most of observed discordance in monazites from amphibolite facies terranes to fluid interaction. Numerous examples of monazites showing patchy zoning characterized by irregular interlocking zones of monazite with variable compositions have been documented (Zhu et al., 1997; Ayers et al., 1999; Zhu and O'Nions, 1999a,b; Townsend et al., 2001). Patchy zoning has been attributed to differential recrystallization or replacement (Stern and Sanborn, 1998; Ayers et al., 1999), to simultaneous intergrowth of monazite with different compositions (Zhu and O'Nions, 1999a), and to leaching of REEs along fractures (Poitrasson et al., 1996). Results from several geochronological studies have found that patchy zones yield younger ages than unaltered zones, most likely caused by partial resetting of the U-Th-Pb system via recrystallization (Hawkins and Bowring, 1997; Townsend et al., 2001). Although compositional zonation is often correlated with age zonation, note that this is not always the case (e.g., Catlos, 2000; Catlos et al., 2002). Because monazite has a low solubility in neutral pH aqueous solutions (Ayers et al., 1999), dissolution-reprecipitation is mostly likely to occur in an environment in which pH evolves from low to neutral values (e.g., Townsend et al., 2001).

Because disturbances to the U-Th-Pb system in monazite are widely reported (indeed, it was once believed that the T_c was 500–600°C; Köppel et al., 1980; Black et al., 1984), mechanisms other than diffusive exchange (e.g., recrystallization, dissolution/reprecipitation) must be relatively common.

4.4.3. Garnet armoring

The resetting of U-Th-Pb ages of matrix monazites compared to those included in coexisting garnets led Montel et al. (2000) to propose that unfractured garnet could armor monazite inclusions against Pb loss to high temperatures (see also Catlos et al., 2002; Gilley et al., 2003). Whether this effect is due to the low solubility of Pb in garnet (Montel et al., 2000) or simply isolating monazite from the dissolution/recrystallization effects (e.g., Hawkins and Bowring, 1997) discussed above is not clear.

4.4.4. Geological closure temperature estimates

Early geological estimates for the closure temperature of Pb in monazite ranged from 530°C (Black et al., 1984) to 600°C (Köppel et al., 1980). However, recent evidence suggests the U-Th-Pb system can remain closed to Pb loss through upper sillimanite zone conditions (Copeland et al., 1988; Smith and Barriero, 1990; Spear and Parrish, 1996). A closure temperature of Pb in monazite was estimated by Copeland et al. (1988)

at 720–750°C for 10–100 μm crystals cooled at 20°C/Ma, based on the presence of inherited monazite in a Himalayan leucogranite. Parrish (1990) suggested a closure temperature of 725 ± 25°C on the basis of a preserved Pb loss profile in monazite from a paragneiss formed under upper amphibolite conditions. Suzuki et al. (1994) calculated closure temperatures for Pb diffusion in monazite as a function of grain size and cooling rate. For a 100 μm monazite, their results indicate closure temperatures of 650°C and 720°C, assuming respective cooling rates of 10 and 100°C/Ma.

More recently, there have been reports that monazite has retained Pb through very high grade metamorphic episodes (e.g., Braun et al., 1998; Cocherie, 1998; Bingen and van Breemen, 1998; Brugier et al., 1999; Kalt et al., 2000; Bosch et al., 2002). For example, Spear and Parrish (1996) observed that conventional U-Pb analyses of bulk monazite from granulite-grade gneiss from the Valhala complex yielded ages as old as 90 Ma despite the fact that it was metamorphosed to 850°C at ca. 63 Ma. They interpreted this as evidence that Pb was relatively immobile under granulite facies conditions. Schmitz and Bowring (2003) reached a similar conclusion for even higher grade granulite xenoliths from kimberlites of the Kaapvaal craton that experienced temperatures in excess of 1000°C for more than 5 Ma. In spite of this, it must be emphasized that inferences regarding Pb retentivity need to be carefully evaluated in light of the potential for garnet to armor monazite inclusions against Pb loss (e.g., Montel et al., 2000). Low solubilities of Pb in garnet may indeed inhibit Pb exchange, and armoring may serve to protect monazites from dissolution/recrystallization effects, but nonetheless the slow diffusivities for Pb in monazite measured in this study, and the calculations in section 4.3, strongly support the contention that the temperature of closure to Pb exchange in monazite can be quite high.

4.4.5. Depth profiling of natural monazites

Another means of evaluating the Pb retentivity of natural monazite involves high resolution examination of Pb gradients adjacent to grain boundaries of geologically heated monazite. Measurable gradients of Pb/Th, interpreted to be due to the loss of Pb, have been observed over sub-μm length scales in natural monazites using a SIMS depth profiling method similar to that described in section 2.4 (e.g., Grove and Harrison, 1999). In cases where observed Pb loss can be attributed to volume diffusion, such gradients contain potentially valuable thermochronological information that can be extracted if the diffusion behavior of Pb in monazite is known. In cases where geological constraints are sufficiently strong, we can use these gradients to determine plausible limits on diffusion behavior, provided that factors other than volume diffusion that might contribute to Pb concentration gradients can be ruled out or their contributions reliably assessed.

Host gneisses in a crystalline nappe studied by Grove and Harrison (1999) experienced peak metamorphic temperatures of 600 to 750°C during the Miocene, but cooled below ca. 400°C by 3 Ma (see summary in Harrison et al., 1999b). Pb/Th depth profiling of monazites from sample DH-68-96, obtained from a 13 Ma cross cutting pegmatite, revealed age gradients within 1 μm of the crystal face, with ~500Å depth resolution.
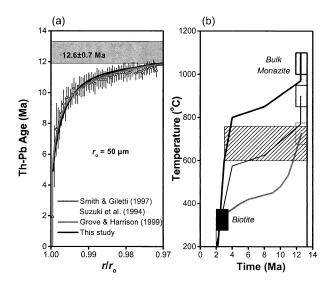
Fig. 10. (a) Th-Pb age profiles in the surface region of monazite DH-68-96. The three curve fits to the data reflect the specific diffusion calibration and thermal history shown in (b), assuming that volume diffusion is solely responsible for the observed profiles. (b) Thermal histories required to fit the Th-Pb age gradient given the three diffusion calibrations shown in (a). Hatched region shows temperature-time region permitted by thermochronometric data. See text for further discussion.

While we cannot unequivocally state that these measured profiles are due solely to volume diffusion of Pb, their continuous nature, the relative conformity of their shape to that expected for radiogenic ingrowth/diffusion loss (Dodson, 1986), and their intergrain consistency effectively rules out protracted growth as an explanation for their formation. Based upon a characteristic transport distance indicated by these profiles of ~0.3 μm (Fig. 10a) and a maximum timescale, τ, at peak temperature of 10 m.y. (i.e., 13–3 Ma; see Fig. 10b), the results imply a value of D_{MAX} of ~5 × 10^{-28} m^2 s^{-1} (via x = $^{1/2}D\tau$). This value is about four orders of magnitude higher than that predicted by our experimentally derived Arrhenius relationship.

Figure 10b shows the temperature histories generated by fitting the observed age gradient with: 1) a diffusion calibration that combines the data of Smith and Giletti (1997) and Suzuki et al. (1994) (180 kJ mol^{-1}; gray curve), and 2) the Arrhenius relationship generated in this study (590 kJ mol^{-1}; thick black curve). Also shown by the thick black curve is the thermal history of a calibration line that passes through the datum estimated from the Grove and Harrison (1999) study ($D_{700°C}$ = 5 × 10^{-28} m^2 s^{-1}) and $D_{1200°C}$ = 10^{-21} m^2 s^{-1} (the only point of agreement shared by both experimental diffusion studies) giving an apparent activation energy of 345 kJ mol^{-1}. It can be seen from Figure 10b that the thermal history predicted from our experimentally determined Arrhenius relationship requires temperatures far in excess of that permissible by the metamorphic constraints. At present, we are not sure why this discrepancy exists. While it is possible that factors other than volume diffusion have contributed to the development of observed Th-Pb age profiles measured by Grove and Harrison (1999), the sharp contrast may signal a change in diffusion mechanism between conditions attainable in the laboratory and in nature. The latter cannot be ruled out, but no evidence of a change in

diffusion mechanism has yet been observed in any study of volume diffusion of cations in minerals over the range of geologically reasonable temperatures. Additional U-Th-Pb depth profiling studies of natural monazites from well-constrained settings may be helpful in clarifying this matter.

5. CONCLUSIONS

1) Diffusion coefficients for Pb in monazite determined for in- and out-diffusion experiments over the temperature range 1100 to 1350°C, analyzed using Rutherford backscattering spectroscopy (RBS), define a linear Arrhenius relationship given by D = 0.94 exp($-592 ± 39$ kJ mol^{-1}/RT) m^2 s^{-1}.

2) Analysis of run products of both in- and out-diffusion experiments by secondary ion mass spectrometry (SIMS) are in general agreement with the RBS results.

3) Both the RBS and SIMS datasets are inconsistent with the results of a Pb diffusion study of a natural monazite by Smith and Giletti (1997) which yielded an activation energy more than three times lower than our result. The explanation for this discrepancy is not completely understood.

4) Extrapolation of our result to geological conditions predicts ultrahigh closure temperatures for Pb in monazite—comparable to those for Pb in zircon. For example, a 20-μm-diameter spherical monazite grain would have a closure temperature of 950°C, given a cooling rate of 10°C/Ma. While inferences regarding the Pb retentivity of monazite are still conflicting, at least some of the results obtained from granulite terranes are consistent with our experimental findings. Additional careful investigations of the ability of garnet to armor monazite against Pb loss (whether through dissolution/recrystallization or diffusion) and well-constrained studies of natural Pb gradients developed adjacent to grain boundaries may be useful in resolving the controversy.

REFERENCES

Anthony J. W. (1957) Hydrothermal synthesis of monazite. *Am. Mineral.* **42,** 904.

Anthony J. W. (1964) An investigation of physical property variations related to thorium content of synthetic monazite. Ph.D. dissertation. Harvard University.

Ayers J. C., Miller C., Gorisch B., and Milleman J. (1999) Textural development of monazite during high-grade metamorphism: Hydrothermal growth kinetics, with implications for U, Th-Pb geochronology. *Am. Mineral.* **84,** 1766–1780.

Bea F. and Montero P. (1999) Behaviour of accessory phases and redistribution of Zr, REE, Y, Th, and U during metamorphism and partial melting of metapelites in the lower crust: An example from the Kinzigite Formation of Ivrea-Verbano, NW Italy. *Geochim. Cosmochim. Acta* **63,** 1133–1153.

Bingen B. and van Breemen O. (1998) U-Pb monazite ages in amphibolite- to granulite-facies orthogneiss reflect hydrous mineral break-

down reactions: Sveconorwegian Province of SW Norway. *Contrib. Mineral. Petrol.* **132,** 336–353.

Black L. P., Fitzgerald J. D., and Harley S. L. (1984) Pb isotopic composition, colour and microstructure of monazites from a poly-metamorphic rock in Antarctica. *Contrib. Mineral. Petrol.* **85,** 141–148.

Bosch D., Hammor D., Bruguier O., Caby R., and Luck J. M. (2002) Monazite "in situ" $^{207}Pb/^{206}Pb$ geochronology using a small geometry high-resolution ion probe: Application to Archean and Proterozoic rocks. *Chem. Geol.* **184,** 151–165.

Braun I., Montel J. M., and Nicollet C. (1998) Electron microprobe dating of monazites from high-grade gneisses and pegmatites of the Kerala Khondalite Belt, southern India. *Chem. Geol.* **146,** 65–85.

Brugier O., Bosch D., Pidgeon R. T., Byrne D. I., and Harris L. B. (1999) U-Pb chronolgy of the Northampton Complex, Western Australia—Evidence for Grenvillian sedimentation, metamorphism and deformation and geodynamic implications. *Contrib. Mineral. Petrol.* **136,** 258–272.

Catlos E. J. (2000) Thermobarometric and geochronologic constraints on the evolution of the Main Central Thrust, Himalayan orogen. PhD dissertation. University of California, Los Angeles.

Catlos E. J., Gilley L. D., and Harrison T. M. (2002) Interpretation of monazite ages obtained via in situ analysis. *Chem. Geol.* **188,** 193–215.

Cherniak D. J. (1993) Lead diffusion in titanite and preliminary results of the effects of radiation damage on Pb transport. *Chem. Geol.* **110,** 177–194.

Cherniak D. J. (1995) Diffusion of lead in plagioclase and K-feldspar: An investigation using Rutherford Backscattering and resonant nuclear reaction analysis. *Contrib. Mineral. Petrol.* **120,** 358–371.

Cherniak D. J. (1997) An experimental study of Sr and Pb diffusion in calcite, and implications for carbonate diagenesis and metamorphism. *Geochim. Cosmochim. Acta* **61,** 4173–4179.

Cherniak D. J. (1998) Pb diffusion in clinopyroxene. *Chem. Geol.* **150,** 105–117.

Cherniak D. J., Lanford W. A., and Ryerson F. J. (1991) Lead diffusion in apatite and zircon using ion implantation and Rutherford Backscattering techniques. *Geochim. Cosmochim. Acta* **55,** 1663–1673.

Cherniak D. J. and Watson E. B. (1992) A study of strontium diffusion in K-feldspar, Na-K feldspar and anorthite using Rutherford Backscattering Spectroscopy. *Earth. Planet. Sci. Lett.* **113,** 411–425.

Cherniak D. J. and Ryerson F. J. (1993) A study of strontium diffusion in apatite using Rutherford Backscattering and ion implantation. *Geochim. Cosmochim. Acta* **57,** 4653–4662.

Cherniak D. J. and Watson E. B. (1994) A study of strontium diffusion in plagioclase using Rutherford Backscattering Spectroscopy. *Geochim. Cosmochim. Acta* **58,** 5179–5190.

Cherniak D. J., Hanchar J. M., and Watson E. B. (1997a) Diffusion of tetravalent cations in zircon. *Contrib. Mineral. Petrol.* **127,** 383–390.

Cherniak D. J., Hanchar J. M., and Watson E. B. (1997b) Rare earth diffusion in zircon. *Chem. Geol.* **134,** 289–301.

Cherniak D. J. and Watson E. B. (2001) Pb Diffusion in zircon. *Chem. Geol.* **172,** 5–24.

Cocherie A. (1998) Geochrology of polygenetic monazites constrained by in situ electron-microprobe Th-U total lead determination—Implications for lead behavior in monazite. *Geochim. Cosmochim. Acta* **62,** 2475–2497.

Copeland P., Parrish R. R., and Harrison T. M. (1988) Identification of inherited radiogenic Pb in monazite and its implications for U-Pb systematics. *Nature* **333,** 760–763.

Crank J. (1975) *The Mathematics of Diffusion.* 2nd ed. Oxford.

Crowley J. L. and Ghent E. D. (1999) An electron microprobe study of the U-Th-Pb systematics of metamorphosed monazite: The role of Pb diffusion versus overgrowth and recrystallization. *Chem. Geol.* **157,** 285–302.

Dahl P. S. (1997) A crystal-chemical basis for Pb retention and fission-track annealing systematics in U-bearing minerals, with implications for geochronology. *Earth Planet. Sci. Lett.* **150,** 277–290.

Derry D. J., Lees D. G., and Calvert J. M. (1981) A study of oxygen self-diffusion in the c-direction of rutile using a nuclear technique. *J. Phys. Chem. Solids* **42,** 57–64.

Dodson M. H. (1973) Closure temperature in cooling geochronological and petrological systems. *Contrib. Mineral. Petrol.* **40,** 259–274.

Dodson M. H. (1986) Closure profiles in cooling systems. *Mater. Sci. Forum.* **7,** 145–154.

Farver J. R. and Giletti B. J. (1998) Strontium diffusion kinetics in apatite. *Eos Trans. Am. Geophys. Union* **79**(Suppl), 369.

Finger F., Broska I., Roberts M. P., and Schermaier A. (1998) Replacement of primary monazite by apatite-allanite-epidote coronas in an amphibolite facies granite gneiss from the eastern Alps. *Am. Mineral.* **83,** 248–258.

Ganguly J., Tirone M., and Hervig R. L. (1998) Diffusion kinetics of samarium and neodymium in garnet, and a method for determining cooling rates of rocks. *Science* **281,** 805–807.

Ganguly J. and Tirone M. (1999) Diffusion closure temperature and age of a mineral with arbitrary extent of diffusion: Theoretical formulation and applications. *Earth Planet. Sci. Lett.* **170,** 131–140.

Giletti B. J. and Casserly J. E. D. (1994) Strontium diffusion kinetics in plagioclase feldspars. *Geochim. Cosmochim. Acta* **58,** 3785–3793.

Gilley L. D., Harrison T. M., Leloup P. H., Ryerson F. J., Lovera O. M., and Wang J. H. (2003) Direct dating of left-lateral deformation along the Red River shear zone, China and Vietnam. *J Geophys. Res.* **108**(B2), 2127.

Gjostein N. A. (1973) *Diffusion.* American Society of Metals.

Grove M. and Harrison T. M. (1999) Monazite Th-Pb age depth profiling. *Geology* **27,** 487–490.

Hammouda T. and Cherniak D. J. (2000) Diffusion of Sr in fluorphlogopite determined by Rutherford Backscattering spectrometry. *Earth. Planet. Sci. Lett.* **178,** 339–349.

Harrison T. M., Ryerson F. J., Le Fort P., Yin A., Lovera O. M., and Catlos E. J. (1997) A Late Miocene-Pliocene origin for the Central Himalayan inverted metamorphism. *Earth Planet. Sci. Lett.* **146,** E1–E8.

Harrison T. M., Grove M., McKeegan K. D., Coath C. D., Lovera O. M., and Le Fort P. (1999a) Origin and episodic emplacement of the Manaslu Intrusive Complex, Central Himalaya. *J. Petrol.* **40,** 3–19.

Harrison T. M., Grove M., Lovera O. M., Catlos E. J., and D'Andrea J. (1999b) The origin of Himalayan anatexis and inverted metamorphism: Models and constraints. *J. Asian Earth Sci.* **17,** 755–772.

Harrison T. M., Catlos E. J. and Montel J.-M. (2002) U-Th-Pb dating of phosphates. In *Phosphates: Geochemical, Geobiological and Materials Importance.* Reviews in Mineralogy and Geochemistry 48, pp. 523–558. Mineralogical Society of America.

Hawkins D. P. and Bowring S. A. (1997) U-Pb systematics of monazite and xenotime: Case studies from the Paleoproterozoic of the Grand Canyon, Arizona. *Contrib. Mineral. Petrol.* **127,** 87–103.

Kalt A., Corfu F., and Wijbrans J. R. (2000) Time calibration of a P-T path from a Variscan high temperature low-pressure metamorphic complex (Bayerische Wald, Germany) and the detection of inherited monazite. *Contrib. Mineral. Petrol.* **138,** 146–163.

Karioris F. G., Gowda K., and Cartz L. (1981) Heavy ion bombardment on monoclinic $ThSiO_4$, ThO_2, and monazite. *Radiat. Eff. Lett.* **58,** 1–3.

Kingsbury J. A., Miller C. F., Wooden J. L., and Harrison T. M. (1993) Monazite paragenesis and U-Pb systematics in rocks of the eastern Mojave Desert, California, USA: Implications for thermochronometry. *Chem. Geol.* **110,** 147–167.

Köppel V., Gunthert A., and Grünenfelder M. (1980) Patterns of U-Pb zircon and monazite ages in polymetamorphic units of the Swiss Central Alps. *Schweiz. Mineral. Petrogr. Mitt.* **61,** 97–119.

Krogstad E. J. and Walker R. J. (1994) High closure temperatures of the U-Pb system in large apatites from the Tin Mountain pegmatite, Black Hills, South Dakota, USA. *Geochim. Cosmochim. Acta* **58,** 3845–3853.

Meldrum A., Wang L. M., and Ewing R. C. (1996) Ion beam induced amorphization of monazite. *Nucl Instr. Meth. Phys. Res. B.* **116,** 220–224.

Meldrum A., Boatner L. A., and Ewing R. C. (1997a) Electron-irradiation-induced nucleation and growth in amorphous $LaPO_4$, $ScPO_4$, and zircon. *J. Mater. Sci.* **12,** 1816–1827.

Meldrum A., Boatner L. A., and Ewing R. C. (1997b) Displacive radiation effects in the monazite- and zircon-structure orthophosphates. *Phys. Rev. B* **56,** 13805–13814.

Meldrum A., Boatner L. A., Weber W. J., and Ewing R. C. (1998) Radiation damage in zircon and monazite. *Geochim. Cosmochim. Acta* **62,** 2509–2520.

Montel J.-M. (1989) Monazite end members and solid solutions: Synthesis, unit-cell characteristics, and utilization as microprobe standards. *Min. Mag.* **53,** 120–123.

Montel J.-M., Kornprobst J., and Vielzeuf D. (2000) Preservation of old U-Th-Pb ages in shielded monazite: Example from the Beni Bousera Hercynian kinzigites (Morocco). *J. Metamorph. Geol.* **18,** 335–342.

Moore D. K., Cherniak D. J., and Watson E. B. (1998) Oxygen diffusion in rutile from 750 to 1000°C and 0.1 to 1000 MPa. *Am. Mineral.* **83,** 700–711.

Murakami T., Chakoumakos B. C., Ewing R. C., Lumpkin G. R., and Weber W. J. (1991) Alpha-decay event damage in zircon. *Am. Mineral.* **76,** 1510–1532.

Parrish R. (1990) U-Pb dating of monazite and its application to geological problems. *Can. J. Earth Sci.* **17,** 1431–1450.

Poitrasson F., Chenery S., and Bland D. J. (1996) Contrasted monazite hydrothermal alteration mechanisms and their geochemical implications. *Earth Planet. Sci. Lett.* **145,** 79–96.

Schmitz M. D. and Bowring S. A. (2003) Ultrahigh-temperature metamorphism in the lower crust during Neoarchean Ventersdorp rifting and magmatism, Kaapvaal Craton, southern Africa. *Geol. Soc. Am. Bull.* **115,** 533–548.

Shestakov G. I. (1969) On diffusional loss of lead from a radioactive mineral. *Geochem. Int.* **6,** 888–896.

Smith H. A. and Barriero B. A. (1990) Monazite U-Pb dating of staurolite grade metamorphism in pelitic schists. *Contrib. Mineral. Petrol.* **105,** 602–615.

Smith H. A. and Giletti B. J. (1997) Lead diffusion in monazite. *Geochim. Cosmochim. Acta* **61,** 1047–1055.

Spear F. S. and Parrish R. R. (1996) Petrology and cooling rates of the Valhalla complex, Br. Columbia, Canada. *J. Petrol.* **37,** 733–765.

Stern R. A. and Sanborn N. (1998) Monazite U-Pb and Th-Ph geochronology by high-resolution secondary ion mass spectrometry. In *Radiogenic Age and Isotopic Studies.* Report 11, pp 1–18. Curr. Res. Geol. Surv. Canada.

Suzuki K., Adachi M., and Kajizuka I. (1994) Electron microprobe observations of Pb diffusion in metamorphosed detrital monazites. *Earth Planet. Sci. Lett.* **128,** 391–405.

Tannhauser D. (1956) Concerning a systematic error in determining diffusion coefficients. *J. Appl. Phys.* **27,** 662.

Teufel S. and Heinrich W. (1997) Partial resetting of the U-Pb isotope system in monazite through hydrothermal experiments: An SEM and U-Pb isotope study. *Chem. Geol.* **137,** 273–281.

Townsend K. J., Miller C. F., D'Andrea J. L., Ayers J. C., Harrison T. M., and Coath C. D. (2001) Low temperature replacement of monazite in the Ireteba granite, Southern Nevada: Geochronological implications. *Chem Geol.* **172,** 95–112.

Watson E. B., Harrison T. M., and Ryerson F. J. (1985) Diffusion of Sm, Sr, and Pb in fluorapatite. *Geochim. Cosmochim. Acta* **49,** 1813–1823.

Watson E. B., Vicenzi E. P., and Rapp R. P. (1989) Inclusion/host relations involving accessory minerals in high-grade metamorphic and anatectic rocks. *Contrib. Mineral. Petrol.* **101,** 220–231.

Watson E. B. and Cherniak D. J. (1997) Oxygen diffusion in zircon. *Earth Planet. Sci. Lett.* **148,** 527–544.

Weber W. J. (1990) Radiation-induced defects and amorphization in zircon. *J. Mater. Res.* **5,** 2687–2697.

Weber W. J., Ewing R. C., and Wang L. M. (1994) The radiation-induced crystalline-to-amorphous transition in zircon. *J. Mater. Res.* **9,** 688–698.

Zhu X. K., O'Nions R. K., Belshaw N. S., and Gibb A. J. (1997) Significance of in situ SIMS chronometry of zoned monazite from the Lewisian Granites, northwest Scotland. *Chem. Geol.* **135,** 35–53.

Zhu X. K. and O'Nions R. K. (1999a) Zonation of monazite in metamorphic rocks and its implications for high-temperature thermochonology: A case study from the Lewisian terrian. *EPSL* **171,** 209–220.

Zhu X. K. and O'Nions R. K. (1999b) Monazite chemical composition: Some implications for monazite geochronology. *Contrib Mineral Petrol.* **137,** 351–363.